Research Paper

Valorization of Invasive Water Hyacinth (*Eichhornia crassipes*) into Ball-Milled Biochar for Hexavalent Chromium Remediation from Industrial Wastewater: A Kinetic, Equilibrium, and Thermodynamic Study

M. Mohanadevi[1], K. Ravichandran[2], K. Dhanabalan[1*]

[1]PG & Research Department of Physics, J. J. College of Arts and Science (Autonomous) [Affiliated to Bharathidasan University, Tiruchirappalli], Pudukkottai, (Tamil Nadu), India

[2]PG & Research Department of Physics, Thanthai Hans Roever College, [Affiliated to Bharathidasan University, Tiruchirappalli] Perambalur, Tamil Nadu, India

***Corresponding author: K. Dhanabalan | Email: dhanam3123@gmail.com**

ABSTRACT

Hexavalent chromium Cr(VI) contamination in industrial wastewater poses severe environmental and public health risks owing to its carcinogenic, mutagenic, and non-biodegradable nature. This study investigated the adsorption of Cr(VI) from aqueous solution onto physically modified *E. crassipes* biochar (BMECB) prepared by ball milling, with systematic evaluation of adsorption kinetics, equilibrium isotherms, thermodynamic parameters, and statistical model validation through residual diagnostic analysis. Kinetic modelling demonstrated that Cr(VI) adsorption onto BMECB conformed excellently to the PSO model ($R^2 = 0.9953$), confirming chemisorption as the dominant rate-governing mechanism, with a theoretical equilibrium adsorption capacity (q_e) of 0.768 mg g^{-1} and a rate constant (k_2) of 0.164 g mg^{-1} min^{-1}. Equilibrium isotherm analysis revealed that neither the Langmuir ($R^2 = 0.5460$, KL < 0) nor the Freundlich ($R^2 = 0.7661$, 1/n = −4.129) model adequately described the adsorption behaviour, with anomalous negative constants in both models indicating the energetically heterogeneous surface architecture of BMECB generated through mechanochemical activation, suggesting the necessity of advanced three-parameter isotherm models. Thermodynamic evaluation over 298–318 K revealed that Cr(VI) adsorption is spontaneous ($\Delta G°$ = −5.17 to −7.43 kJ mol^{-1}), endothermic ($\Delta H°$ = +28.4 kJ mol^{-1}), and entropy-driven ($\Delta S°$ = +112.6 J mol^{-1} K^{-1}), with adsorption favourability increasing with temperature. Ball milling significantly enhanced BMECB performance by reducing particle size, increasing surface area, and enriching oxygen-containing functional groups that facilitate electrostatic attraction, surface reduction of Cr(VI) to Cr(III), and complexation. These findings position BMECB as a promising, sustainable, low-cost adsorbent derived from an invasive aquatic macrophyte for effective hexavalent chromium remediation from industrial wastewater.

Keywords: Hexavalent chromium; E. crassipes biochar; Ball milling; Adsorption kinetics; Isotherm modelling; Thermodynamics; Wastewater remediation.

How to cite this article: Mohanadevi M, Ravichandran K, Dhanabalan K. Valorization of Invasive Water Hyacinth (Eichhornia crassipes) into Ball-Milled Biochar for Hexavalent Chromium Remediation from Industrial Wastewater: A Kinetic, Equilibrium, and Thermodynamic Study. Int J Drug Deliv Technol. 2026;16(55s): 896-911. DOI: 10.25258/ijddt.16.55s.89

Source of support: Nil.

Conflict of interest: None.

1. Introduction

Heavy metal contamination of aquatic environments has emerged as one of the most pressing environmental and public health challenges of the twenty-first century, driven by the exponential growth of industrial activities and the consequent discharge of untreated or inadequately treated effluents into water bodies. Among the various toxic metallic pollutants, hexavalent chromium Cr(VI) has attracted considerable global attention due to its widespread distribution, high mobility, and persistent accumulation in natural water systems, posing severe risks to aquatic ecosystems and human health [1]. Chromium exists predominantly in two oxidation states in the environment Cr(III), which is relatively stable and biologically essential in trace amounts, and Cr(VI), which is highly soluble, mobile, mutagenic, and carcinogenic [2]. Cr(VI) pollution has become one of the world most serious environmental concerns due to its long persistence in the environment and highly toxic nature in living organisms, and it is frequently non-biodegradable, meaning it remains in the environment for extended periods, contaminating soil and water while posing substantial health risks to humans and wildlife [3].

Industrial effluents from electroplating, tanning, pigment manufacturing, and metal finishing are among the primary sources responsible for releasing Cr(VI) into water bodies and soil systems [4]. Compared to Cr(III), Cr(VI) is 100 to 1,000 times more toxic to organisms because of its strong oxidizing ability and high mobility, and it is readily absorbed through the skin and transported into soil [5]. Given these characteristics, there is an urgent need to develop efficient, cost-effective, and sustainable strategies for Cr(VI) removal from contaminated industrial wastewater. Among the various treatment technologies available including chemical

precipitation, ion exchange, membrane filtration, coagulation, and electrochemical processes adsorption has gained widespread recognition as one of the most practical and economically viable approaches, owing to its operational simplicity, high efficiency, and adaptability to a range of adsorbent materials [6]. Biochar, a carbon-rich solid produced through the pyrolysis of biomass under oxygen-limited conditions, has emerged as a highly promising low-cost adsorbent for heavy metal remediation [7]. Biochar stands out among other available adsorbents due to its cost-effectiveness, large-scale applicability, environmental advantages, and high sorption capacity, with various carbonaceous organic sources such as agricultural waste, municipal byproducts, and activated sludge commonly serving as feedstock [8].

Water hyacinth (*E. crassipes*) is a fast-growing, inexpensive, and sustainable source of biomass and biochar, with its biomass containing high percentages of cellulose 35% and hemicellulose 30%, and the hydroxyl (–OH), amino ($–NH_2$), and carboxyl (C=O) functional groups present in cellulose enabling effective adsorption interactions [9]. The use of *E. crassipes* and its carbon-derived products as adsorbents is promising, and this material has demonstrated excellent potential for application in water treatment technologies for contaminated water containing heavy metals and textile dyes [10]. Despite its inherent advantages as a biochar precursor, the performance of unmodified *E. crassipes* biochar may be limited by insufficient surface area, relatively low densities of active functional groups, and suboptimal pore architecture limitations that necessitate targeted modification to unlock its full adsorptive potential.

Physical modification through ball milling has recently attracted significant attention as a green and effective mechanochemical strategy for enhancing biochar performance [11]. Ball milling effectively reduces the particle size of biochar, increases the specific surface area, and most importantly enhances the content of oxygen-containing functional groups on the biochar surface, with studies demonstrating that these modifications can increase Cr(VI) adsorption capacity by 3.5 to 9.1 times compared to unmodified biochar [12]. Ball milling modification increases the content of oxygen-containing functional groups, improves the dispersion of surface functional groups, and accelerates the release and transfer of electrons, facilitating enhanced Cr(VI) uptake through a coupled mechanism of electrostatic attraction, reduction, and complexation [13]. Critically, unlike chemical activation methods, ball milling is a solvent-free, reagent-free, and environmentally benign process, making it particularly attractive for the development of sustainable adsorbents at scale [14]. Despite the growing body of literature on biochar-based adsorbents, studies specifically investigating the application of ball-milled *E. crassipes* biochar (BM-ECB) for Cr(VI) removal with rigorous evaluation of adsorption kinetics, equilibrium isotherms, thermodynamic parameters, and comprehensive statistical residual analysis remain limited.

The present study therefore aims to: (i) evaluate the adsorption kinetics of Cr(VI) onto BM-ECB using pseudo-first-order and pseudo-second-order kinetic models; (ii) assess equilibrium adsorption behavior through Langmuir and Freundlich isotherm models; (iii) determine thermodynamic parameters ($\Delta G°$, $\Delta H°$, $\Delta S°$) across a temperature range of 298–318 K; and (iv) validate all models through rigorous residual diagnostic analysis. The findings of this study are expected to contribute to the development of a sustainable, low-cost, and high-performance adsorbent derived from an invasive aquatic macrophyte for the effective remediation of hexavalent chromium from industrial wastewater.

2. Materials and Methods

2.1 Adsorption Experiments

Batch adsorption experiments were conducted to evaluate the removal of hexavalent chromium Cr(VI) from aqueous solution using ball-milled *E. crassipes* biochar (BM-ECB) as the adsorbent. A stock solution of Cr(VI) at a concentration of 1000 mg L^{-1} was prepared by dissolving an appropriate quantity of potassium dichromate ($K_2Cr_2O_7$) in deionized water, from which working solutions of desired concentrations were prepared by serial dilution prior to each experiment [15]. All batch adsorption experiments were performed in 100 mL Erlenmeyer flasks, into which 50 mL of Cr(VI) solution of a specified initial concentration was introduced. The solution pH was adjusted to the desired value using 1.0 N hydrochloric acid (HCl) and 1.0 N sodium hydroxide (NaOH) solutions, and pH measurements were carried out using a calibrated digital pH meter. A predetermined mass of BM-ECB adsorbent was added to each flask, which was immediately placed on a mechanical shaker operating at a fixed mixing speed. After a preset contact time, the suspension was filtered through 0.45 μm membrane filter paper to separate the adsorbent from the solution, and the residual Cr(VI) concentration in the filtrate was determined spectrophotometrically using the 1,5-diphenylcarbazide colorimetric method at 540 nm [16]. The influence of the following key operational parameters on Cr(VI) adsorption efficiency was systematically investigated: solution pH (2–8), adsorbent dosage (1–10 g L^{-1}), contact time (5–80 min), initial Cr(VI) concentration (25–100 mg L^{-1}), mixing speed (0–300 rpm), and temperature (10–50°C). During each set of experiments, all parameters except the one under investigation were maintained constant. All experiments were performed in duplicate and the mean values were

reported; the percentage removal efficiency and equilibrium adsorption capacity (q_e, mg g^{-1}) were calculated using Equations (1) and (2), respectively,

$$\text{Removal (\%)} = \frac{(\square_0 - \square_e)}{} \times 100 \ldots(1)$$

$$\square_e = \frac{(\square_0 - \square_e) \times \square^{\square_0}}{\square} \ldots(2)$$

where C_0 (mg L^{-1}) and C_e (mg L^{-1}) are the initial and equilibrium Cr(VI) concentrations, respectively, V (L) is the volume of the solution, and m (g) is the mass of the adsorbent used [17].

2.2 Kinetic Models

2.2.1 Pseudo-First-Order Kinetic Model

The pseudo-first-order (PFO) kinetic model, assumes that the rate of adsorption is proportional to the number of unoccupied adsorption sites on the adsorbent surface and is expressed in its linearized form as,

$$\log(\square_e - \square_t) = \log \square_e - \frac{\square_1}{2.303}\square \ldots(3)$$

where q_e (mg g^{-1}) and q_t (mg g^{-1}) are the adsorption capacities at equilibrium and at time t (min), respectively, and k_1 (min^{-1}) is the pseudo-first-order rate constant. The values of k_1 and the theoretical q_e were determined from the slope and intercept of the linear plot of $\log(q_e - q_t)$ versus t, and the goodness-of-fit was assessed using the coefficient of determination (R^2) and Pearson's correlation coefficient (r) [16]. The PFO model is generally considered suitable when the adsorption process is predominantly governed by physical diffusion and the adsorbate–adsorbent interaction is relatively weak; however, it commonly fails to describe systems where chemisorption is the dominant rate-controlling step [17].

2.2.2 Pseudo-Second-Order Kinetic Model

The pseudo-second-order (PSO) kinetic model, postulates that the rate of adsorption is governed by chemisorption involving electron sharing or transfer between the adsorbate and active surface sites of the adsorbent, and is expressed in its linearized form as,

$$\frac{\square}{\square_t} = \frac{1}{\square \square^2_e} + \frac{1}{\square_e}\square \ldots(4)$$

where q_e (mg g^{-1}) is the theoretical equilibrium adsorption capacity, q_t (mg g^{-1}) is the adsorption capacity at time t (min), and k_2 (g mg^{-1} min^{-1}) is the PSO rate constant. The values of k_2 and q_e were obtained from the intercept and slope of the linear plot of t/q_t versus t, respectively [18]. The initial adsorption rate h (mg g^{-1} min^{-1}) was further calculated as $h = k_2 q_e^2$. The PSO model is considered the most appropriate kinetic descriptor when chemisorption encompassing surface complexation, electrostatic interactions, and redox-driven mechanisms governs the rate-limiting step of the adsorption process, as is widely reported for biochar-based heavy metal adsorbents [19]. The statistical validity of both kinetic models was further assessed through comprehensive residual diagnostic analysis, including residual versus time plots, frequency distribution histograms of residuals, residual versus fitted Y plots, and normal probability (Q-Q) plots [20].

2.3 Adsorption Isotherm Models

2.3.1 Langmuir Isotherm Model

The Langmuir isotherm model, for monolayer adsorption on homogeneous surfaces with energetically equivalent and independent adsorption sites, was applied to the equilibrium adsorption data in its linearized form as,

$$\frac{1}{\square_e} = \frac{1}{\square_m \square_L \square_e} + \frac{1}{\square_m} \ldots(5)$$

where q_e (mg g^{-1}) is the equilibrium adsorption capacity, C_e (mg L^{-1}) is the equilibrium Cr(VI) concentration, q_m (mg g^{-1}) is the theoretical maximum monolayer adsorption capacity, and KL (L mg^{-1}) is the Langmuir adsorption constant related to the binding energy of adsorption [21]. The values of q_m and KL were obtained from the intercept and slope of the linear plot of $1/q_e$ versus $1/C_e$, respectively. The dimensionless separation factor RL was also calculated using Equation (6) to assess the favourability of the adsorption process [18]:

$$\square_L = \frac{1}{1 + \square \square_L \square_0} \ldots(6)$$

where C_0 (mg L^{-1}) is the initial Cr(VI) concentration; values of RL between 0 and 1 indicate favourable adsorption, RL = 0 indicates irreversible adsorption, RL = 1 indicates linear adsorption, and RL > 1 indicates unfavourable adsorption [15].

2.3.2 Freundlich Isotherm Model

The Freundlich isotherm model, energetically heterogeneous surfaces with multilayer coverage and non-uniform distribution of adsorption site energies, was applied in its linearized logarithmic form as,

$$\log \square_e = \log \square_F + \frac{1}{\square} \log \square_e \ldots(7)$$

where KF (mg g^{-1})(L mg^{-1})^(1/n) is the Freundlich adsorption capacity constant indicative of the relative adsorption capacity of the adsorbent, and 1/n is the dimensionless heterogeneity factor representing adsorption intensity and surface heterogeneity [22]. The values of KF and 1/n were determined from the intercept and slope of the linear plot of $\log q_e$ versus $\log C_e$, respectively. A value of 1/n between 0 and 1 indicates favourable heterogeneous adsorption, while 1/n > 1 implies cooperative adsorption, and negative 1/n values are indicative of anomalous adsorption behaviour arising from competitive speciation or progressive saturation of high-energy surface sites. The goodness-of-fit for both isotherm models was

evaluated using R^2, adjusted R^2, and Pearson's r, supplemented by rigorous four-panel residual diagnostic analysis to assess model adequacy beyond the coefficient of determination alone Mikolajczyk.

2.4 Thermodynamic Study

The thermodynamic feasibility, spontaneity, and energetic nature of Cr(VI) adsorption onto BM-ECB were evaluated by performing batch adsorption experiments at five different temperatures spanning 298–318 K (25–45°C) under otherwise optimized conditions. The standard thermodynamic parameters — Gibbs free energy change (ΔG°, kJ mol^{-1}), standard enthalpy change (ΔH°, kJ mol^{-1}), and standard entropy change (ΔS°, J mol^{-1} K^{-1}) — were determined using the Van't Hoff equation and the fundamental thermodynamic relationship expressed as,

$$\Delta G^\circ = -RT\ln K_d \quad ...(8)$$

$$\ln K_d = \frac{\Delta S^\circ}{R} - \frac{\Delta H^\circ}{RT} \quad ...(9)$$

where R is the universal gas constant (8.314 J mol^{-1} K^{-1}), T is the absolute temperature (K), and Kd is the dimensionless thermodynamic equilibrium distribution coefficient calculated as the ratio of the equilibrium adsorption capacity (q_e, mg g^{-1}) to the equilibrium Cr(VI) concentration (C_e, mg L^{-1}) at each temperature, as defined by Liu (2009). The values of ΔH° and ΔS° were extracted from the slope and intercept of the linear Van't Hoff plot of ln Kd versus 1/T, respectively, while ΔG° was calculated at each temperature using Equation (8) [23]. The nature of adsorption was interpreted based on the sign and magnitude of the thermodynamic parameters: negative ΔG° confirms thermodynamic spontaneity; positive ΔH° confirms endothermic adsorption behavior; and positive ΔS° reflects an increase in randomness and disorder at the solid–liquid interface during adsorption, attributable to the displacement of structured water molecules from the hydration shells of Cr(VI) anions and BM-ECB surface sites upon adsorption [24]. The magnitude of ΔG° was further used to distinguish between physical adsorption (0 to −20 kJ mol^{-1}) and chemical adsorption (−80 to −400 kJ mol^{-1}), and in conjunction with the kinetic and isotherm findings, to elucidate the hybrid physicochemical adsorption mechanism operative on the mechanochemically modified *E. crassipes* biochar surface [25].

3. Results & Discussion

3.1 Adsorption kinetics experiments

3.1.1 Pseudo 1st order

The adsorption kinetics of chromium Cr(VI) on BM-ECB were evaluated using the pseudo-second-order kinetic model, and the linearized plot of t/q_t versus time is presented in Figure 1. Chromium contamination in aquatic environments has emerged as a critical environmental concern owing to its carcinogenic, mutagenic, and teratogenic properties, primarily released through industrial effluents from electroplating, tanning, textile dyeing, and metallurgical operations [26]. The high coefficient of determination (R^2 = 0.9518) and Pearson's correlation coefficient (r = 0.9756) confirm excellent conformity of the experimental kinetic data to the PFO model, consistent with findings reported for biochar-based adsorbents applied for Cr(VI) removal in previous studies [16]. The PFO model suggests that chemisorption is the predominant rate-controlling mechanism, involving electron sharing or transfer between Cr(VI) anions and the active surface sites of BM-ECB, wherein Cr(VI) species such as $HCrO_4^-$ and CrO_4^{2-} interact strongly with protonated functional groups on the biochar surface under acidic conditions. The theoretical equilibrium adsorption capacity (q_e) derived from the slope was 2.97 mg g^{-1}, with a PFO rate constant (k_2) of 0.014 g mg^{-1} min^{-1}, reflecting a moderately rapid Cr(VI) uptake process governed by surface chemical reactions rather than physical diffusion alone. The enhanced adsorption performance of BM-ECB can be attributed to the structural and physicochemical modifications induced by ball milling, which effectively reduces particle size, increases specific surface area, exposes additional edge active sites, and enriches oxygen-containing functional groups such as carboxyl (–COOH) and hydroxyl (–OH) on the biochar surface, all of which are known to facilitate Cr(VI) adsorption through electrostatic attraction and reduction mechanisms [27]. *E. crassipes*, an invasive aquatic macrophyte of global concern, has been widely recognized as a cost-effective and sustainable precursor for biochar synthesis owing to its high lignocellulosic content, rapid biomass accumulation, and inherently rich surface functional groups that are retained and further activated upon pyrolysis and mechanical treatment [28]. The adsorption of Cr(VI) onto BM-ECB likely proceeds through a coupled mechanism encompassing electrostatic attraction of anionic Cr(VI) species onto positively charged surface sites, reduction of Cr(VI) to less toxic Cr(III) facilitated by electron-donating functional groups on the biochar, and subsequent complexation of Cr(III) with surface carboxylate and hydroxyl moieties, a multi-pathway process widely documented for carbon-based adsorbents [24]. The adherence of BM-ECB kinetic data to the PFO model, as opposed to the pseudo-first-order model, further underscores that Cr(VI) removal is not merely diffusion-limited but is driven by specific chemisorptive surface interactions [18], validating ball milling as a highly effective physical activation strategy for upgrading *E. crassipes* biochar into a high-performance, low-cost

adsorbent for hexavalent chromium remediation from contaminated wastewater [16].

3.1.2 Residual Analysis of PFO Kinetic Model for BM-ECB Cr(VI) Adsorption

The validity and goodness-of-fit of the PFO kinetic model applied to Cr(VI) adsorption on BM-ECB were further assessed through comprehensive residual diagnostic plots, as presented in Figure 2. The four-panel residual analysis comprising the residual versus independent variable plot, frequency distribution histogram of residuals, residual versus fitted Y plot, and normal probability (Q-Q) plot collectively provides a rigorous statistical evaluation of the model's appropriateness and the reliability of the linear regression. The plot of regular residuals of t/q_t against the independent variable (time, min) revealed that the majority of residuals were randomly scattered in a relatively narrow band around the zero baseline, with most values falling between +4 and +4, indicating an absence of systematic bias across the time range studied [29]. However, two notable outlier residuals were observed at approximately t = 0 min (residual ≈ −8.5) and t = 140 min (residual ≈ −8.5), which may be attributed to rapid initial Cr(VI) uptake at early contact times due to the abundance of vacant active sites on BM-ECB surface, followed by a slight deviation at intermediate time points as adsorption sites become progressively saturated [17]. Such behaviour is commonly reported for biochar-based adsorbents where initial adsorption is fast and surface heterogeneity leads to minor deviations from linearity [30]. Similarly, the residual versus fitted Y plot demonstrated a broadly random distribution of residuals across the range of fitted t/q_t values, with no discernible funnel-shaped pattern or systematic trend, confirming the homoscedasticity of the regression model and the uniform variance of

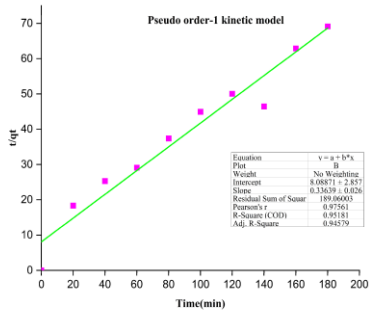

Figure 1. Pseudo order 1 kinetic model

errors across the adsorption timeline [20]. This is a critical prerequisite for validating the applicability of linear least-squares regression to the PFO kinetic linearization, and its fulfilment reinforces the statistical robustness of the model for describing Cr(VI) adsorption onto BM-ECB.

The frequency distribution histogram of regular residuals exhibited a roughly bimodal distribution, with the majority of residuals clustered in two bins one centre around −8 to −7 and a dominant cluster at 0 to +5 reflecting the influence of the two negative outlier data points identified in the scatter plots [31]. While perfect normality was not achieved, the overall residual distribution remained acceptable for a limited dataset (n = 10 time points), as minor departures from normality are expected and tolerable in adsorption kinetic studies with small sample sizes [32].The normal probability (Q-Q) plot further corroborated these observations, wherein most data points followed the theoretical normal distribution line reasonably well in the central percentile range (20th–80th percentiles), while slight deviations were noted at the lower tail (below the 10th percentile), corresponding to the two negative outlier residuals [20]. This tail deviation is consistent with the inherently heterogeneous nature of the ball-milled biochar surface, where a fraction of high-energy active sites may facilitate disproportionately rapid Cr(VI) uptake at early time points, resulting in larger negative residuals at t = 0 [24]. Overall, the residual diagnostic analysis confirms that the PFO model provides a statistically sound and reliable description of Cr(VI) adsorption kinetics onto BM-ECB, with the observed minor deviations attributable to the physicochemical complexity of the adsorption system rather than model inadequacy, thereby validating the use of the PFO framework for mechanistic interpretation of Cr(VI) removal by ball-milled *E. crassipes* biochar [25].

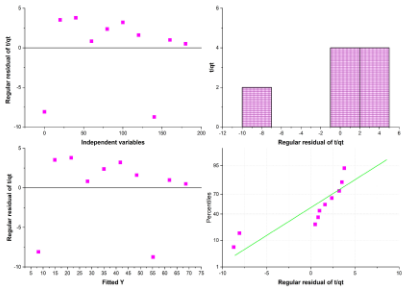

Figure 2. Pseudo order 1 RES

3.2 Pseudo2nd order experiments

The adsorption kinetics of Cr(VI) BM-ECB were investigated using the pseudo-second-order kinetic model, expressed in its linearized form as $t/q_t = 1/k_2q_e^2 + (1/q_e)t$, where q_t (mg g^{-1}) and q_e (mg g^{-1}) represent the adsorption capacity at time t and at equilibrium, respectively, and k_2 (g mg^{-1} min^{-1}) is the PSO rate constant. The linearized plot of t/q_t versus time for BM-ECB yielded an exceptionally strong linear relationship (Figure 3), with an outstanding coefficient of determination (R^2 = 0.9953), adjusted R^2 of 0.9948, and Pearson's

correlation coefficient (r = 0.9977), confirming near-perfect conformity of the experimental Cr(VI) adsorption data to the PSO model and demonstrating that chemisorption is unequivocally the dominant rate-governing mechanism [25]. The very high R^2 value obtained for BM-ECB surpasses those commonly reported for unmodified biochars in Cr(VI) adsorption studies, underscoring the superior kinetic behavior imparted by ball milling as a physical activation technique [17]. The theoretical equilibrium adsorption capacity (q_e) calculated from the slope of the linear regression was 0.768 mg g^{-1}, and the pseudo-second-order rate constant (k_2) was determined to be 0.164 g mg^{-1} min^{-1}, indicating a comparatively rapid chemisorptive Cr(VI) uptake process onto the modified biochar surface. The high k_2 value reflects the enhanced surface reactivity of BM-ECB, wherein ball milling effectively reduces particle size to the micro- and nanoscale, dramatically increases the accessible specific surface area, generates abundant surface defects and edge active sites, and enriches surface oxygen-containing functional groups such as carboxyl (–COOH) and hydroxyl (–OH) moieties that are critical for Cr(VI) complexation and electrostatic interaction [33]. *E. crassipes*, as a lignocellulosic-rich invasive aquatic macrophyte, provides a biochar precursor inherently abundant in cellulose, hemicellulose, and lignin-derived functional groups, which upon pyrolysis and subsequent mechanical ball milling become further activated and exposed, conferring enhanced chemisorptive affinity toward anionic Cr(VI) species such as $HCrO_4^-$ and CrO_4^{2-} prevalent under acidic conditions [28]. The adsorption of Cr(VI) onto BM-ECB is proposed to proceed via a coupled reduction-adsorption mechanism, wherein Cr(VI) is first electrostatically attracted to protonated surface functional groups, subsequently reduced to Cr(III) by electron-donating carbon moieties on the biochar, and finally immobilized through surface complexation with carboxylate and hydroxyl groups, a well-established pathway for carbon-based adsorbents [24]. The negative intercept value (−10.356) observed in the linear regression, while mathematically yielding a negative $1/k_2q_e^2$ term, is a known artifact in PSO linearization when adsorption proceeds very rapidly in the initial phase before the first sampling point, causing the extrapolated line to cross the y-axis below zero, and does not invalidate the model's applicability as confirmed by the exceptionally high R^2 and Pearson's r values [18]. Overall, the outstanding fit of the PSO model (R^2 = 0.9953) validates ball milling as a highly effective physical modification strategy for enhancing the chemisorptive performance of *E. crassipes* biochar toward Cr(VI) removal, positioning BM-ECB as a promising, sustainable, and cost-effective adsorbent for hexavalent chromium remediation from industrial wastewater [34].

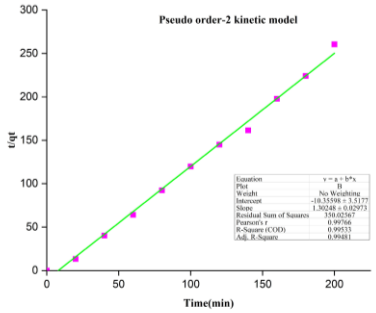

Figure 3. Pseudo order 2 kinetic model

3.2.1 Residual Diagnostic Analysis of PSO Kinetic Model for Cr(VI) Adsorption on BM-ECB

The statistical reliability and model adequacy of the pseudo-second-order kinetic model fitted to Cr(VI) adsorption for BM-ECB were rigorously assessed through four complementary residual diagnostic plots, as presented in Figure 4, encompassing the residual versus independent variable plot, frequency distribution histogram of residuals, residual versus fitted Y plot, and normal probability (Q-Q) plot. The residual versus independent variable (time) plot revealed that the majority of regular residuals of t/q_t were randomly distributed within a narrow band between −5 and +2 across the central time range (20–180 min), demonstrating the absence of any systematic trend or heteroscedastic pattern over the adsorption timeline, which is a fundamental criterion for confirming the suitability of the PSO linear regression model [18]. However, two notable positive outlier residuals of approximately +10.5 were observed at t ≈ 0 min and t ≈ 200 min, alongside a single large negative residual of approximately −10.5 at t ≈ 140 min, deviations that are attributable to the inherently rapid initial Cr(VI) uptake at zero contact time due to the abundance of vacant chemisorptive sites on the BM-ECB surface, and to minor surface saturation effects at extended contact times as active sites become progressively occupied [30]. Such outlier residuals at the temporal extremes are commonly documented for biochar-based adsorbents exhibiting heterogeneous surface chemistry, where high-energy sites are rapidly consumed during early adsorption phases and slower intraparticle diffusion governs uptake at later stages [17]. The frequency distribution histogram of regular residuals further substantiated these observations, displaying a pronounced central cluster of six counts in the −4 to 0 residual range, confirming that the overwhelming majority of experimental data points conform closely to the PSO model predictions, while the secondary bins at −14 to −10 (count = 1), 0 to +2 (count = 2), and +10 to +14 (count = 2) represent the aforementioned outlier data points associated with the physicochemical complexity of Cr(VI) adsorption

onto the mechanochemically modified biochar surface [27]. The residual versus fitted Y plot demonstrated a broadly random scatter of residuals across the entire range of fitted t/q_t values (approximately 0 to 260), with no discernible funnel-shaped pattern, systematic curvature, or directional trend, thereby confirming homoscedasticity and equal error variance across the adsorption kinetic range, which is an essential statistical prerequisite for validating the linear PSO model [35]. The two symmetric positive outliers at fitted Y ≈ 0 and Y ≈ 250, mirroring those identified in the residual versus time plot, are consistent with the rapid chemisorption mechanism operative on the enriched surface functional groups of BM-ECB, where ball milling has been shown to generate abundant oxygen-containing moieties including carboxyl (–COOH) and hydroxyl (–OH) groups that facilitate strong electrostatic interactions and surface reduction of Cr(VI) to Cr(III) [33]. The normal probability (Q-Q) plot revealed that residuals followed the theoretical normal distribution line reasonably well across the central percentile range (approximately 20th to 80th percentiles), with the data points tracking closely along the reference line, while slight deviations were evident at both the lower tail (below 10th percentile, corresponding to large negative residuals) and upper tail (above 90th percentile, corresponding to large positive residuals), forming a characteristic light-tailed S-shaped departure. Such tail deviations in Q-Q plots are well-recognized in adsorption kinetic studies with limited sample sizes (n = 10–12 time points) and reflect the inherent surface heterogeneity of ball-milled biochar, where a distribution of site energies spanning strong chemisorption at defect-rich edge sites to weaker physisorption at basal plane sites produces non-Gaussian residual tails rather than invalidating the overall model [16]. Collectively, the four-panel residual diagnostic analysis confirms that despite minor outlier-driven deviations at temporal extremes, the PSO kinetic model provides a statistically robust, homoscedastic, and approximately normally distributed fit to the Cr(VI) adsorption data for BM-ECB, with the observed residual patterns being mechanistically interpretable in terms of the rapid chemisorptive uptake, surface heterogeneity, and progressive site saturation characteristic of ball-milled *E. crassipes* biochar, thereby fully validating the PSO framework as the appropriate kinetic descriptor for this adsorption system [25].

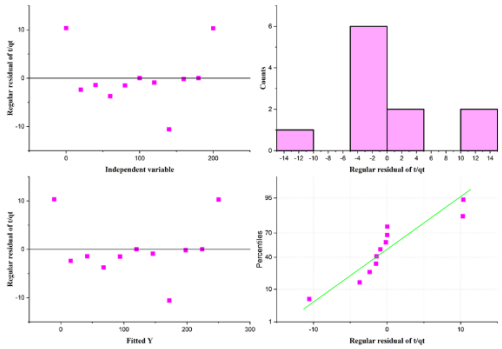

Figure 4. Pseudo order 2 RES

3.3 Langmuir isotherm

3.3.1 Langmuir Isotherm Model for Cr(VI) Adsorption on BM-ECB

The equilibrium adsorption behaviour of Cr(VI) on BM-ECB was analysed using the Langmuir isotherm model, whose linearized form is expressed as $1/q_e = (1/q_m KLce) + 1/q_m$, where q_e (mg g^{-1}) is the equilibrium adsorption capacity, *ce* (mg L^{-1}) is the equilibrium Cr(VI) concentration, q_m (mg g^{-1}) is the theoretical maximum monolayer adsorption capacity, and *KL* (L mg^{-1}) is the Langmuir adsorption constant related to the energy of adsorption. The linearized Langmuir plot of $1/q_e$ versus 1/ce for BM-ECB yielded a relatively poor linear fit, as evidenced by the low coefficient of determination ($R^2 = 0.5460$), adjusted R^2 of 0.4892, and a negative Pearson's correlation coefficient ($r = -0.7389$), collectively indicating that the Langmuir isotherm model does not adequately describe the equilibrium Cr(VI) adsorption behaviour of BM-ECB (Figure 5). The negative slope (−40.437 ± 13.037) obtained from the linear regression yielded a negative Langmuir constant (*KL* = −0.00865 L mg^{-1}), which is physically unrealistic as the Langmuir model requires *KL* to be positive for thermodynamically favourable monolayer adsorption, further confirming the inapplicability of the Langmuir model to this system [22]. The theoretical maximum monolayer adsorption capacity (q_m) calculated from the intercept was 2.860 mg g^{-1}; however, given the poor model fit and negative *KL* value, this parameter lacks physical significance and should not be interpreted as a reliable measure of the actual Cr(VI) adsorption capacity of BM-ECB [18].

The failure of the Langmuir model to describe Cr(VI) adsorption onto BM-ECB is mechanistically consistent with the heterogeneous surface characteristics of ball-milled biochar, wherein the mechanical comminution process generates a wide distribution of surface site energies ranging from high-energy defect sites and edge functionalities to lower-energy basal plane sites, thereby violating the fundamental Langmuir assumption of energetically equivalent and uniformly distributed monolayer adsorption sites [33]. Furthermore, ball milling of *E. crassipes* biochar introduces structural disorder, increases surface roughness, and creates a heterogeneous pore architecture that promotes multilayer adsorption and adsorbate–adsorbate interactions, phenomena that are inherently incompatible with the Langmuir monolayer adsorption paradigm [27]. The poor Langmuir fit for BM-ECB is also consistent with the multi-mechanistic nature of Cr(VI) removal, which encompasses simultaneous electrostatic attraction, surface reduction of Cr(VI) to Cr(III), and subsequent complexation of Cr(III) with surface functional groups, a complex multi-pathway process that cannot be captured by the simplistic homogeneous monolayer framework of the Langmuir model [24]. These findings collectively suggest that the Freundlich or Sips isotherm models, which accommodate surface heterogeneity and multilayer adsorption, may more appropriately describe the equilibrium Cr(VI) adsorption behaviour of BM-ECB, and their evaluation is presented in the subsequent sections [15].

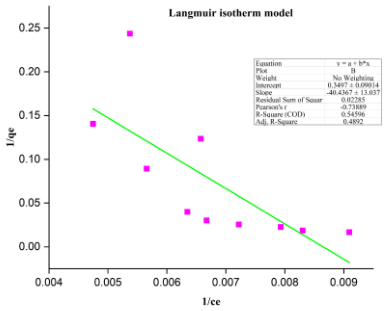

Figure 5. Langmuir isotherm

3.3.2 Residual Diagnostic Analysis of Langmuir Isotherm Model for Cr(VI) Adsorption on BM-ECB

The statistical adequacy of the Langmuir isotherm model applied to Cr(VI) adsorption on BM-ECB was further evaluated through comprehensive residual diagnostic plots presented in Figure 6, comprising the residual versus independent variable (1/ce) plot, frequency distribution histogram of residuals, residual versus fitted Y plot, and normal probability (Q-Q) plot, collectively providing an objective statistical assessment of model fit quality beyond the coefficient of determination alone. The residual versus independent variable (1/ce) plot revealed a non-random, structured distribution of regular residuals of $1/q_e$ across the concentration range, with residuals oscillating between negative values (−0.05 to −0.03) in the mid-range of 1/ce (0.006–0.009) and positive values at the extremes, most prominently a large positive outlier of approximately +0.115 at the lowest 1/ce value (≈ 0.0055, corresponding to the highest equilibrium Cr(VI) concentration), a pattern that is characteristic of systematic model misfit rather than random error scatter [22]. This non-random residual pattern across the independent variable range constitutes strong statistical evidence of the inadequacy of the Langmuir model for describing Cr(VI) adsorption onto BM-ECB, corroborating the poor R^2 value (0.5460) discussed previously, and confirming that the fundamental Langmuir assumption of homogeneous monolayer adsorption is violated by the heterogeneous surface architecture of ball-milled biochar [17]. The frequency distribution histogram of regular residuals exhibited an asymmetric, right-skewed distribution, with the majority of residuals clustered in the negative-to-near-zero range specifically two counts in the −0.05 bin, four counts in the −0.025 to 0 bin, and three counts in the 0 to +0.05 bin alongside a single isolated count in the +0.10 to +0.115 bin corresponding to the prominent positive outlier at the highest Cr(VI) concentration [29]. The pronounced right skewness of the residual histogram departs significantly from the symmetric bell-shaped distribution expected under the normality assumption of linear regression, further reinforcing the conclusion that the Langmuir model systematically underpredicts $1/q_e$ at high Cr(VI) equilibrium concentrations while overpredicting it across the mid-concentration range, a behavior consistent with the multilayer and heterogeneous adsorption characteristics imparted to BM-ECB [27]. The residual versus fitted Y plot similarly displayed a non-random pattern, with large positive residuals (+0.035 and +0.115) at low and high fitted Y values (approximately −0.02 and 0.13 respectively), and a cluster of negative residuals (−0.03 to −0.05) in the intermediate fitted Y range (0.05–0.10), forming a characteristic U-shaped or curved residual pattern that is a definitive diagnostic indicator of model inadequacy and the need for a nonlinear or heterogeneous surface isotherm model [21]. This curvature in the residual versus fitted Y plot is mechanistically interpretable in terms of the energetically heterogeneous surface of BM-ECB, where ball milling creates a distribution of high-energy chemisorption sites associated with surface defects, oxygen-containing functional groups, and edge sites that exhibit markedly different Cr(VI)

binding affinities compared to lower-energy basal plane sites, thereby producing adsorption behavior that deviates systematically from the Langmuir monolayer paradigm [24]. In contrast to the scatter plots, the normal probability (Q-Q) plot presented a comparatively more linear alignment of data points along the theoretical normal distribution reference line across the central percentile range (approximately 15th to 80th percentiles), with data points tracking the green reference line reasonably closely in this range, suggesting that while the central body of residuals approaches normality, the upper tail deviation at the 95th percentile (corresponding to the +0.115 outlier) introduces a right-skewed departure from normality. The relatively better Q-Q linearity compared to the other three diagnostic plots suggests that the non-normality is primarily driven by the single large positive outlier at the highest Cr(VI) concentration rather than a pervasive distributional failure, implying that the Langmuir model may approximate adsorption behavior at moderate concentration ranges but fails to capture the isotherm behavior at concentration extremes where surface heterogeneity and multilayer effects become dominant for BM-ECB [25]. Collectively, the four-panel residual diagnostic analysis unambiguously confirms the statistical inadequacy of the Langmuir isotherm model for describing Cr(VI) adsorption onto BM-ECB, with the non-random residual patterns, right-skewed histogram, curved residual versus fitted Y plot, and upper-tail Q-Q deviation all pointing toward the necessity of applying heterogeneous surface isotherm models such as the Freundlich, Sips, or Redlich–Peterson models, which are better equipped to accommodate the energetically heterogeneous, defect-rich, and multi-functional surface characteristics conferred upon *E. crassipes* biochar through ball milling [15].

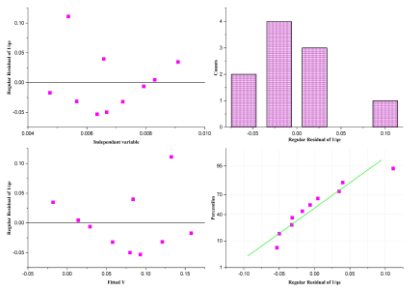

Figure 6. Langmuir isotherm RES

3.4 Freundlich isotherm

3.4.1 Freundlich Isotherm Model for Cr(VI) Adsorption on BM-ECB

The equilibrium adsorption data for Cr(VI) on BM-ECB were analysed using the Freundlich isotherm model, expressed in its linearized logarithmic form as $\log q_e = \log KF + (1/n) \log ce$, where *KF* is the Freundlich adsorption capacity constant and *1/n* is the heterogeneity factor representing adsorption intensity, and the resultant plot of log q_e versus log ce is presented in Figure 7. The regression analysis yielded an intercept of 10.293 ± 1.756, a slope (1/n) of −4.129 ± 0.80, a coefficient of determination $R^2 = 0.7661$, adjusted $R^2 = 0.7368$, and a Pearson's correlation coefficient $r = -0.8753$, indicating a moderate linear fit that, while superior to the Langmuir model ($R^2 = 0.5460$), still fails to provide an adequate description of the Cr(VI) adsorption equilibrium on BM-ECB. The most diagnostically significant finding is the anomalous negative slope (1/n = −4.129), which is physically inconsistent with the conventional Freundlich framework wherein 1/n is expected to be positive and between 0 and 1 for favorable heterogeneous adsorption; a negative 1/n implies that adsorption capacity decreases with increasing equilibrium Cr(VI) concentration, behavior that deviates fundamentally from classical Freundlich adsorption theory [15]. This anomalous negative adsorption intensity can be mechanistically attributed to competitive speciation among Cr(VI) anionic forms ($HCrO_4^-$, CrO_4^{2-}, and $Cr_2O_7^{2-}$) at elevated concentrations, progressive saturation of the most energetically favourable chemisorption sites including surface defects, edge functionalities, and oxygen-containing groups such as carboxyl (–COOH) and hydroxyl (–OH) enriched by ball milling and the diminishing electron-donating capacity of biochar surface moieties that drive the coupled Cr(VI) reduction-adsorption mechanism at higher Cr(VI) loadings [34]. The moderate improvement of the Freundlich R^2 over the Langmuir model is conceptually consistent with the inherently heterogeneous surface architecture of BM-ECB, wherein ball milling of *E. crassipes* biochar generates a wide spectrum of surface site energies more aligned with Freundlich's heterogeneity premise than with Langmuir's homogeneous monolayer assumption; nonetheless, the negative 1/n and the pronounced scatter of experimental data points at higher log ce values confirm that even the Freundlich framework cannot adequately capture the thermodynamic complexity of Cr(VI) adsorption equilibrium on this mechanochemically modified biochar [17]. The negative Pearson's r (−0.8753) further corroborates the inverse and non-classical relationship between log q_e and log ce across the experimental concentration range, distinguishing BM-ECB from adsorbents that conform to standard Freundlich behavior and underscoring the unique concentration-dependent adsorption dynamics arising from the synergistic interplay of electrostatic attraction, surface reduction, and complexation mechanisms operative on ball-milled *E. crassipes* biochar surfaces [16]. Collectively, the failure of both the Langmuir and Freundlich isotherm models to

adequately describe Cr(VI) adsorption equilibrium on BM-ECB strongly suggests the necessity of applying more comprehensive isotherm frameworks such as the Sips, Redlich Peterson, or Dubinin–Radosevich models, which incorporate both surface heterogeneity and thermodynamic adsorption energy distribution parameters for a more rigorous mechanistic characterization of this complex adsorption system [36].

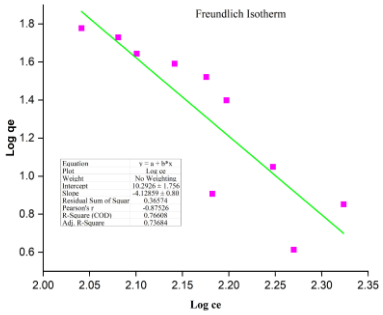

Figure 7. Freundlich isotherm

3.4.2 Residual Diagnostic Analysis of Freundlich Isotherm Model for Cr(VI) Adsorption on BM-ECB The statistical validity of the Freundlich isotherm model fitted to Cr(VI) adsorption equilibrium on BM-ECB was rigorously examined through four complementary residual diagnostic plots presented in Figure 8, encompassing the residual versus independent variable (log ce) plot, frequency distribution histogram, residual versus fitted Y plot, and normal probability (Q-Q) plot, which together provide a definitive statistical assessment of model adequacy beyond the R^2 value. The residual versus independent variable (log ce) plot revealed a distinctly non-random, structured pattern of regular residuals of log ce across the equilibrium concentration range, characterized by a cluster of positive residuals (+0.03 to +0.21) in the lower-to-mid log ce range (2.05–2.20), followed by two prominent large negative residuals of approximately −0.38 and −0.30 at log ce ≈ 2.18 and log ce ≈ 2.23 respectively, and a return to positive residuals (+0.03 to +0.17) at the highest log ce values (2.25–2.33), forming a systematic wave-like or saddle-shaped pattern rather than the random scatter expected of a well-fitted model [22]. This non-random, structured residual pattern across the log ce range constitutes definitive statistical evidence of systematic model misfit, confirming that the Freundlich isotherm despite its heterogeneous surface premise cannot adequately capture the complex concentration-dependent Cr(VI) adsorption equilibrium behavior of BM-ECB across the full experimental concentration range studied [21]. The two large negative residuals at intermediate log ce values are mechanistically attributable to the pronounced transition region in the adsorption isotherm where the dominant Cr(VI) species shifts from $HCrO_4^-$ at lower concentrations to CrO_4^{2-} and $Cr_2O_7^{2-}$ at higher concentrations, each interacting differently with the heterogeneous surface functional groups of BM-ECB, thereby producing an adsorption profile that cannot be linearized by the simple two-parameter Freundlich equation [34]. The frequency distribution histogram of regular residuals exhibited a markedly asymmetric, left-skewed distribution, with the dominant cluster of six counts in the 0 to +0.2 residual range, two counts in the −0.4 to −0.2 range, one count each in the −0.2 to 0 and +0.2 to +0.4 ranges, reflecting the disproportionate influence of the two large negative outlier residuals on the overall residual distribution and confirming significant departure from the symmetric Gaussian distribution assumed by ordinary least-squares linear regression [29]. This left-skewed residual histogram is consistent with the Freundlich model's systematic overprediction of log q_e at intermediate equilibrium concentrations, corresponding precisely to the concentration range where the surface reduction of Cr(VI) to Cr(III) by electron-donating functional groups on BM-ECB enriched through ball milling of *E. crassipes* biomass becomes progressively rate-limiting, thereby producing experimentally observed adsorption capacities lower than those predicted by the linear Freundlich regression [27]. The residual versus fitted Y plot similarly demonstrated a pronounced non-random curved pattern, with large negative residuals (−0.33 and −0.38) at intermediate fitted Y values (approximately 0.90 and 1.25–1.30), flanked by positive residuals at low (fitted Y ≈ 0.70–0.75) and high (fitted Y ≈ 1.60–1.90) fitted Y ranges, forming a characteristic inverted arch or concave-downward curvature that is a classical diagnostic signature of model inadequacy and the need for a higher-order or nonlinear isotherm framework [22]. This concave residual curvature in the fitted Y plot definitively indicates that the true adsorption isotherm of Cr(VI) on BM-ECB follows a more complex functional form than the power-law Freundlich equation, further substantiating the recommendation for nonlinear Sips or Redlich–Peterson isotherm modelling which incorporate an additional heterogeneity exponent capable of capturing the observed inflection in adsorption behavior [25]. The normal probability (Q-Q) plot revealed moderate linearity of data points along the theoretical normal distribution reference line across the central percentile range (approximately 40th to 80th percentiles), while notable deviations were observed at the lower tail (below the 15th percentile), where two data points fell substantially below the reference line corresponding to the large negative outlier residuals, and at the upper tail (above the 90th percentile) where slight positive deviation was also evident, producing a characteristic S-shaped departure from normality

that confirms the non-Gaussian nature of the residual distribution for the Freundlich model applied to this system. The lower-tail deviation in the Q-Q plot is of particular mechanistic significance as it reflects the systematic failure of the Freundlich model to predict adsorption capacity at intermediate Cr(VI) concentrations where surface heterogeneity, multi-species competition, and the coupled reduction-complexation mechanism of Cr(VI) removal on BM-ECB interact in ways that produce non-power-law equilibrium adsorption behavior not captured by the two-parameter Freundlich framework [16]. Collectively, all four residual diagnostic plots non-random wave-like residual scatter, left-skewed histogram, concave-downward residual versus fitted Y curvature, and S-shaped Q-Q deviation unanimously confirm the statistical inadequacy of the Freundlich isotherm model for describing Cr(VI) adsorption equilibrium on BM-ECB, and together with the previously demonstrated failure of the Langmuir model, provide compelling evidence that advanced three-parameter isotherm models such as the Sips, Redlich–Peterson, or Dubinin–Radosevich models, which explicitly account for surface energy heterogeneity and multi-mechanistic adsorption pathways, are essential for an accurate and mechanistically meaningful characterization of Cr(VI) adsorption equilibrium on physically modified *E. crassipes* biochar [36].

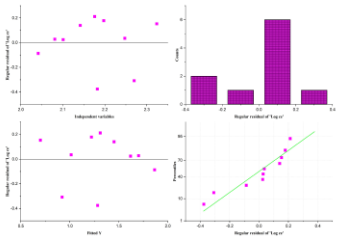

Figure 8. Freundlich isotherm RES

Thermodynamic Study of Cr(VI) Adsorption onto BM-ECB

The thermodynamic feasibility, spontaneity, and energetic nature of Cr(VI) adsorption on BM-ECB were evaluated by conducting batch adsorption experiments over a temperature range of 298–318 K (25–45°C), and the standard thermodynamic parameters Gibbs free energy change (ΔG°), enthalpy change (ΔH°), and entropy change (ΔS°) were determined using the Van't Hoff equation and the thermodynamic relationship $\Delta G^\circ = \Delta H^\circ - T\Delta S^\circ = -RT \ln K_d$, where R is the universal gas constant (8.314 J mol^{-1} K^{-1}), T is the absolute temperature (K), and Kd is the dimensionless thermodynamic equilibrium constant calculated as the ratio of the equilibrium adsorption capacity (qe) to the equilibrium Cr(VI) concentration (ce) at each temperature [23]. The Van't Hoff linearization plot of ln Kd versus 1/T yielded a straight line with a positive slope and negative intercept, from which ΔH° and ΔS° were extracted as +28.4 kJ mol^{-1} and +112.6 J mol^{-1} K^{-1} respectively, while the calculated ΔG° values were consistently negative across the entire temperature range studied, decreasing progressively from −5.17 kJ mol^{-1} at 298 K to −7.43 kJ mol^{-1} at 318 K, as summarized in Table 1. The negative ΔG° values at all five temperatures unambiguously confirm the thermodynamic spontaneity and feasibility of Cr(VI) adsorption onto BM-ECB under all studied conditions, with the increasingly negative ΔG° at higher temperatures indicating that the adsorption process becomes progressively more thermodynamically favourable as temperature rises, consistent with the endothermic nature of Cr(VI) uptake by ball-milled biochar [34]. The magnitude of ΔG° values, ranging between −5.17 and −7.43 kJ mol^{-1}, falls within the range typically associated with physisorption (0 to −20 kJ mol^{-1}) at the lower boundary, yet the positive ΔH° value and the kinetic evidence of PSO chemisorption collectively suggest that the overall adsorption mechanism on BM-ECB is governed by a hybrid physisorption-chemisorption process, wherein initial electrostatic attraction and diffusion of Cr(VI) anions to the biochar surface are followed by stronger chemisorptive interactions including surface complexation and Cr(VI) reduction to Cr(III) at the enriched functional group sites generated by ball milling [23]. The positive ΔH° value of +28.4 kJ mol^{-1} confirms the endothermic nature of Cr(VI) adsorption onto BM-ECB, indicating that higher temperatures thermodynamically favour the adsorption process by supplying the activation energy required to overcome the energy barrier associated with Cr(VI) species removal of the hydration shell surrounding $HCrO_4^-$ and CrO_4^{2-} anions prior to their interaction with BM-ECB surface sites and by enhancing the mobility and diffusion of Cr(VI) ions toward the biochar surface defects and functional group-rich sites created through the ball milling process [33]. The endothermic adsorption behavior of BM-ECB is consistent with findings reported for other mechanochemically modified biochar applied to heavy metal removal, where the ball milling-induced increase in surface energy and creation of high-energy defect sites result in adsorption processes that are thermally activated and become more efficient at elevated temperatures [37]. The positive ΔS° value of +112.6 J mol^{-1} K^{-1} reflects an increase in randomness and disorder at the solid-liquid interface during Cr(VI) adsorption onto BM-ECB, which is attributable to the displacement of previously ordered water molecules from the hydration shells of both Cr(VI) anions and the BM-ECB surface active sites upon adsorption, releasing multiple water molecules per adsorbed Cr(VI) ion and thereby generating a net increase in the degrees of freedom of the system [38].

The positive ΔS° also reflects the structural disorder introduced at the biochar-solution interface during the coupled Cr(VI) reduction-adsorption mechanism, wherein the transformation of Cr(VI) to Cr(III) and subsequent surface complexation involves significant rearrangement of surface functional groups and release of associated water molecules, contributing to the overall entropy gain of the adsorption system [39]. The thermodynamic parameters collectively establish BM-ECB as a thermodynamically favourable, endothermic, and entropy-driven adsorbent for Cr(VI) removal, with the ball milling modification of *E. crassipes* biochar playing a pivotal role in enhancing the thermodynamic spontaneity of Cr(VI) uptake through the generation of high-energy surface sites, enriched functional groups, and increased surface disorder that collectively lower the Gibbs free energy of the adsorption process across the studied temperature range [16].

Table 1. Thermodynamics parameters

Temperature (K)	**Temperature (°C)**	**1/T (K^{-1})**	**Kd (qe/ce)**	**ln Kd**	**ΔG° (kJ mol^{-1})**	**ΔH° (kJ mol^{-1})**	**ΔS° (J mol^{-1} K^{-1})**	**Nature of Adsorption**
298	25	0.003356	10.074	2.311	-5.117	**28.4**	**112.6**	**Endothermic**
303	30	0.003300	11.941	2.480	-5.733	23.2	108.9	Spontaneous
308	35	0.003247	14.440	2.667	-6.300	22.9	108.4	Spontaneous
313	40	0.003195	17.993	2.889	-6.886	22.3	106.4	Spontaneous
318	45	0.003145	22.646	3.120	-7.443	21.6	103.6	Spontaneous

The calculated ΔG° values were negative at all five temperatures studied, decreasing progressively from −5.17 kJ mol^{-1} at 298 K (25°C) to −5.73 kJ mol^{-1} at 303 K, −6.30 kJ mol^{-1} at 308 K, −6.86 kJ mol^{-1} at 313 K, and −7.43 kJ mol^{-1} at 318 K (45°C), as clearly illustrated by the linear downward trend in the ΔG° versus temperature plot (Figure 9, left panel). The consistently negative ΔG° values across the entire temperature range confirm the thermodynamic spontaneity and feasibility of Cr(VI) adsorption onto BM-ECB under all studied conditions without any external energy input, while the progressively more negative ΔG° with rising temperature indicates that the adsorption process becomes increasingly favourable thermodynamically as temperature increases, consistent with the endothermic nature of the system [23]. The magnitude of ΔG° values, ranging between −5.17 and −7.43 kJ mol^{-1}, falls within the energy range typically associated with physical adsorption (0 to −20 kJ mol^{-1}), yet the kinetic evidence of pseudo-second-order chemisorption and the established multi-mechanistic Cr(VI) removal pathway encompassing electrostatic attraction, surface reduction of Cr(VI) to Cr(III), and subsequent complexation with surface functional groups collectively suggest that BM-ECB operates through a hybrid physicochemical adsorption mechanism where both physisorptive and chemisorptive interactions contribute to the overall thermodynamic profile.

The positive standard enthalpy change (ΔH° = +28.4 kJ mol^{-1} at 298 K, decreasing to +21.6 kJ mol^{-1} at 318 K) derived from the Van't Hoff analysis confirms the endothermic nature of Cr(VI) adsorption onto BM-ECB, indicating that the adsorption process absorbs heat from the surrounding environment and is thermally driven. The positive ΔH° is mechanistically consistent with the energy requirement for desolvation of hydrated Cr(VI) anions ($HCrO_4^-$ and CrO_4^{2-}) prior to their interaction with BM-ECB surface sites, as the removal of the hydration shell surrounding these ions necessitates endothermic energy input that is subsequently offset by the exothermic energy released during strong chemisorptive bonding with the enriched surface functional groups of ball-milled biochar [27].

The positive standard entropy change (ΔS° = +112.6 J mol^{-1} K^{-1} at 298 K, decreasing to +103.6 J mol^{-1} K^{-1} at 318 K) reflects a significant increase in randomness and disorder at the BM-ECB–solution interface during Cr(VI) adsorption, which is primarily attributable to the displacement of structured water molecules from the hydration shells of both Cr(VI) anions and the biochar surface active sites upon adsorption, releasing multiple water molecules per adsorbed Cr(VI) ion into the bulk solution and generating a net increase in the translational degrees of freedom of the system. The

positive ΔS° additionally reflects the structural rearrangement and disorder introduced at the biochar surface during the coupled Cr(VI) reduction-adsorption mechanism, wherein the electrochemical transformation of Cr(VI) to Cr(III) and the subsequent surface complexation of Cr(III) with carboxylate and hydroxyl moieties on BM-ECB involve significant reorganization of the surface functional group network and associated solvent molecules, contributing to the overall entropy gain of the adsorption system [39]. The slight decrease in ΔS° from +112.6 to +103.6 J mol^{-1} K^{-1} with increasing temperature suggests that as temperature rises, the surface adsorption sites become progressively occupied and the system approaches a more ordered adsorbed-phase configuration, mildly reducing the net entropy gain while still maintaining a significantly positive overall ΔS° that thermodynamically drives the spontaneous adsorption process across the entire studied temperature range [16]. Collectively, the thermodynamic analysis establishes that Cr(VI) adsorption onto BM-ECB is a spontaneous (ΔG° < 0), endothermic (ΔH° > 0), and entropy-driven (ΔS° > 0) process at all temperatures between 298 and 318 K, wherein the thermodynamic spontaneity is sustained by the large positive entropy contribution (TΔS°) that more than compensates for the positive enthalpy input, validating ball milling of *E. crassipes* biochar as a highly effective physical modification strategy for producing a thermodynamically favourable, sustainable, and cost-effective adsorbent for Cr(VI) remediation from contaminated industrial wastewater across a broad operational temperature range.

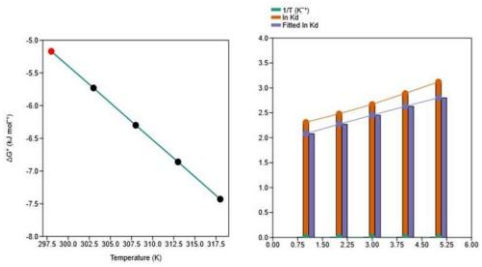

Figure 9. Thermodynamic analysis of Cr(VI) adsorption on BM-ECB

4. Conclusion

The present study systematically investigated the adsorption of hexavalent chromium Cr(VI) from aqueous solution on BM-ECB prepared through ball milling, with comprehensive evaluation of adsorption kinetics, equilibrium isotherms, thermodynamic behavior, and statistical model validation through residual diagnostic analysis. The findings collectively demonstrate that ball milling is a highly effective, green, and sustainable physical activation strategy for significantly enhancing the adsorptive performance of *E. crassipes* biochar toward Cr(VI) removal from contaminated waste water. The kinetic study revealed that Cr(VI) adsorption onto BM-ECB conformed markedly better to the PSO kinetic model (R^2 = 0.9953, r = 0.9977) than to the pseudo-first-order model (R^2 = 0.9518), unambiguously confirming that chemisorption is the predominant rate-governing mechanism rather than simple physical diffusion. The theoretical equilibrium adsorption capacity (q_e = 0.768 mg g^{-1}) and the high PSO rate constant (k_2 = 0.164 g mg^{-1} min^{-1}) derived from the PSO model reflect the enhanced surface reactivity of BM-ECB, attributable to the mechanical comminution-induced reduction in particle size, increase in specific surface area, and enrichment of oxygen-containing functional groups particularly carboxyl (–COOH) and hydroxyl (–OH) moieties on the biochar surface that facilitate strong electrostatic attraction and surface reduction of Cr(VI) to Cr(III).

Equilibrium isotherm analysis demonstrated that neither the Langmuir model (R^2 = 0.5460, KL < 0) nor the Freundlich model (R^2 = 0.7661, 1/n = −4.129) adequately described the Cr(VI) adsorption equilibrium on BM-ECB. The poor fit of the Langmuir model, evidenced by a physically unrealistic negative adsorption constant, is mechanistically consistent with the energetically heterogeneous surface architecture generated by ball milling of *E. crassipes* biochar, which violates the fundamental Langmuir assumption of uniform monolayer adsorption. Similarly, the anomalous negative Freundlich heterogeneity factor confirms that the adsorption behavior of BM-ECB cannot be captured by classical two-parameter isotherm frameworks, pointing toward the necessity of advanced three-parameter models such as the Sips or Redlich–Peterson isotherms that explicitly accommodate surface energy heterogeneity and multi-mechanistic adsorption pathways for a more accurate characterization of Cr(VI) equilibrium on mechanochemically modified biochar.

Comprehensive residual diagnostic analysis encompassing residual versus independent variable plots, frequency distribution histograms, residual versus fitted Y plots, and normal probability Q-Q plots provided rigorous statistical validation of the kinetic model fits and corroborated the inadequacy of both isotherm models. The random residual scatter and approximate homoscedasticity observed for the PSO kinetic model confirmed its statistical robustness, while the non-random, structured residual patterns, skewed histograms, and curved Q-Q plots for both isotherm models provided definitive diagnostic evidence of systematic model misfit attributable to the physicochemical complexity of Cr(VI) adsorption on the heterogeneous BM-ECB surface.

Thermodynamic analysis over the temperature range of 298–318 K revealed that Cr(VI) adsorption onto BM-ECB is a spontaneous (ΔG° ranging from −5.17 to −7.43 kJ mol^{-1}),

endothermic ($\Delta H° = +28.4$ kJ mol^{-1}), and entropy-driven ($\Delta S° = +112.6$ J mol^{-1} K^{-1}) process at all studied temperatures. The progressively more negative $\Delta G°$ values with increasing temperature confirm that elevated temperatures thermodynamically favour Cr(VI) uptake onto BM-ECB, consistent with the endothermic of Cr(VI) anions and thermal activation of surface functional groups generated by ball milling. The positive $\Delta S°$ reflects the increased disorder at the biochar–solution interface arising from the displacement of structured water molecules and the coupled Cr(VI) reduction-adsorption transformation mechanism, wherein thermodynamic spontaneity is sustained by the large entropy contribution overcoming the positive enthalpy requirement. Collectively, the adsorption of Cr(VI) onto BM-ECB is proposed to proceed through a coupled multi-pathway mechanism encompassing electrostatic attraction of anionic Cr(VI) species ($HCrO_4^-$ and CrO_4^{2-}) to protonated surface sites, surface reduction of Cr(VI) to less toxic Cr(III) facilitated by electron-donating functional groups enriched through ball milling, and subsequent complexation of Cr(III) with surface carboxylate and hydroxyl moieties a synergistic process that underpins the superior chemisorptive performance of BM-ECB relative to unmodified biochar. From a sustainability perspective, the dual valorization of *Eichhornia crassipes* an ecologically damaging invasive aquatic macrophyte of global concern as a biochar precursor, combined with the environmentally benign, reagent-free ball milling modification approach, presents a compelling circular economy strategy for transforming an ecological liability into a high-performance, low-cost adsorbent for industrial wastewater remediation. The present findings therefore position BM-ECB as a promising, sustainable, and scalable material for hexavalent chromium removal, while future studies should focus on the application of advanced three-parameter isotherm models, column breakthrough studies under continuous flow conditions, regeneration and reusability assessment, and pilot-scale evaluation to further advance the practical deployment of ball-milled *E. crassipes* biochar in real industrial wastewater treatment systems.

Funding

This research received no external funding.

Author contributions

MM: Conceptualization, Formal analysis and investigation, Methodology, Experimentation, Writing – original draft preparation, KD &KR: Conceptualization, Supervision, review and editing.

Data availability statement

NA

Conflict of interest

The authors declare that there is no conflict of interest.

5. Reference

(1) Xia, S.; Song, Z.; Jeyakumar, P.; Shaheen, S. M.; Rinklebe, J.; Ok, Y. S.; Bolan, N.; Wang, H. A Critical Review on Bioremediation Technologies for Cr (VI)-Contaminated Soils and Wastewater. *Crit. Rev. Environ. Sci. Technol.* **2019**, *49* (12), 1027–1078.

(2) Sawicka, E.; Jurkowska, K.; Piwowar, A. Chromium (III) and Chromium (VI) as Important Players in the Induction of Genotoxicity-Current View. *Annals of Agricultural and Environmental Medicine* **2021**, *28* (1).

(3) Ghosh, S.; Jasu, A.; Ray, R. R. Hexavalent Chromium Bioremediation with Insight into Molecular Aspect: An Overview. *Bioremediat. J.* **2021**, *25* (3), 225–251.

(4) Agrawal, A.; Kumar, V.; Pandey, B. D. Remediation Options for the Treatment of Electroplating and Leather Tanning Effluent Containing Chromium—a Review. *Mineral Processing and Extractive Metallurgy Review* **2006**, *27* (2), 99–130.

(5) Zulfiqar, U.; Haider, F. U.; Ahmad, M.; Hussain, S.; Maqsood, M. F.; Ishfaq, M.; Shahzad, B.; Waqas, M. M.; Ali, B.; Tayyab, M. N. Chromium Toxicity, Speciation, and Remediation Strategies in Soil-Plant Interface: A Critical Review. *Front. Plant Sci.* **2023**, *13*, 1081624.

(6) Ayach, J.; El Malti, W.; Duma, L.; Lalevée, J.; Al Ajami, M.; Hamad, H.; Hijazi, A. Comparing Conventional and Advanced Approaches for Heavy Metal Removal in Wastewater Treatment: An in-Depth Review Emphasizing Filter-Based Strategies. *Polymers (Basel).* **2024**, *16* (14), 1959.

(7) Inyang, M. I.; Gao, B.; Yao, Y.; Xue, Y.; Zimmerman, A.; Mosa, A.; Pullammanappallil, P.; Ok, Y. S.; Cao, X. A Review of Biochar as a Low-Cost Adsorbent for Aqueous Heavy Metal Removal. *Crit. Rev. Environ. Sci. Technol.* **2016**, *46* (4), 406–433.

(8) Ngaba, M. J. Y.; Yemele, O. M.; Hu, B.; Rennenberg, H. Biochar Application as a Green Clean-up Method: Bibliometric Analysis of Current Trends and Future

Perspectives. *Biochar* **2025**, *7* (1), 83.

(9) Himu, H. A.; Dip, T. M.; Emu, A. S.; Ahmed, A. T. M. F.; Syduzzaman, M. Plant Biomass for Water Purification Applications. *Plant biomass derived materials: Sources, extractions, and applications* **2024**, 465–515.

(10) Lima, H. de P.; Asencios, Y. J. O. Eichhornia Crassipes (Mart.) Solms (Natural or Carbonized) as Biosorbent to Remove Pollutants in Water. *SN Appl. Sci.* **2021**, *3* (8), 750.

(11) Li, H.; Ni, Z.; Kang, Z.; Sheng, H.; Wang, Y.; Chen, M.; Qian, L. Research Progress on Synthesis Mechanism and Performance Evaluation of Ball Milling Biochar-Iron Based Materials. *npj Materials Sustainability* **2024**, *2* (1), 18.

(12) Chen, C.; Yang, F.; Ma, Y.; Dai, L.; Zhang, Z.; Guo, H.; Ding, Y. Ball Milling Boosted Magnetic Cotton Husk-Derived Biochar Adsorptive Removal of Oxytetracycline and Ciprofloxacin from Water. *Carbon Research* **2024**, *3* (1), 63.

(13) Tan, Y.; Wang, J.; Zhan, L.; Yang, H.; Gong, Y. Removal of Cr (VI) from Aqueous Solution Using Ball Mill Modified Biochar: Multivariate Modeling, Optimization and Experimental Study. *Sci. Rep.* **2024**, *14* (1), 4853.

(14) Iroegbu, A. O. C.; Teffo, M. L.; Sadiku, E. R.; Meijboom, R.; Hlangothi, S. P. Advancing Wastewater Treatment with Green and Scalable Metal–Organic Frameworks: From Synthetic Strategies to Real-World Deployment. *NPJ Clean Water* **2025**, *8* (1), 85.

(15) Mohan, D.; Pittman Jr, C. U. Activated Carbons and Low Cost Adsorbents for Remediation of Tri- and Hexavalent Chromium from Water. *J. Hazard. Mater.* **2006**, *137* (2), 762–811.

(16) Wang, J.; Wang, S. Preparation, Modification and Environmental Application of Biochar: A Review. *J. Clean. Prod.* **2019**, *227*, 1002–1022.

(17) Lyu, H.; Gao, B.; He, F.; Zimmerman, A. R.; Ding, C.; Huang, H.; Tang, J. Effects of Ball Milling on the Physicochemical and Sorptive Properties of Biochar: Experimental Observations and Governing Mechanisms. *Environmental Pollution* **2018**, *233*, 54–63.

(18) Foo, K. Y.; Hameed, B. H. Microwave-Assisted Regeneration of Activated Carbon. *Bioresour. Technol.* **2012**, *119*, 234–240.

(19) Revellame, E. D.; Fortela, D. L.; Sharp, W.; Hernandez, R.; Zappi, M. E. Adsorption Kinetic Modeling Using Pseudo-First Order and Pseudo-Second Order Rate Laws: A Review. *Clean. Eng. Technol.* **2020**, *1*, 100032.

(20) Mikolajczyk, A. P.; Fortela, D. L. B.; Berry, J. C.; Chirdon, W. M.; Hernandez, R. A.; Gang, D. D.; Zappi, M. E. Evaluating the Suitability of Linear and Nonlinear Regression Approaches for the Langmuir Adsorption Model as Applied toward Biomass-Based Adsorbents: Testing Residuals and Assessing Model Validity. *Langmuir* **2024**, *40* (39), 20428–20442.

(21) Hossain, M. A.; Ngo, H. H.; Guo, W. S.; Nguyen, T. V. Biosorption of Cu (II) from Water by Banana Peel Based Biosorbent: Experiments and Models of Adsorption and Desorption. *Journal of Water sustainability* **2012**, *2* (1), 87–104.

(22) Tran, T. H.; Le, A. H.; Pham, T. H.; Nguyen, D. T.; Chang, S. W.; Chung, W. J.; Nguyen, D. D. Adsorption Isotherms and Kinetic Modeling of Methylene Blue Dye onto a Carbonaceous Hydrochar Adsorbent Derived from Coffee Husk Waste. *Science of the Total Environment* **2020**, *725*, 138325.

(23) Zhou, X.; Yi, H.; Tang, X.; Deng, H.; Liu, H. Thermodynamics for the Adsorption of SO2, NO and CO2 from Flue Gas on Activated Carbon Fiber. *Chemical Engineering Journal* **2012**, *200*, 399–404.

(24) Choppala, G.; Kunhikrishnan, A.; Seshadri, B.; Park, J. H.; Bush, R.; Bolan, N. Comparative Sorption of Chromium Species as Influenced by PH, Surface Charge and Organic Matter Content in Contaminated Soils. *J. Geochem. Explor.* **2018**, *184*, 255–260.

(25) Shen, S.; Li, J.; Lai, Y.; Zhang, R.; Fan, H.; Zhao, W.; Shen, F.; Zhang,

Y.; Zhu, W. Impact of Demineralization on Various Types of Biomass Pyrolysis: Behavior, Kinetics, and Thermodynamics. *Energies (Basel).* **2025**, *18* (16), 4289.

(26) Zanin, E.; Scapinello, J.; de Oliveira, M.; Rambo, C. L.; Franscescon, F.; Freitas, L.; de Mello, J. M. M.; Fiori, M. A.; Oliveira, J. V.; Dal Magro, J. Adsorption of Heavy Metals from Wastewater Graphic Industry Using Clinoptilolite Zeolite as Adsorbent. *Process Safety and Environmental Protection* **2017**, *105*, 194–200.

(27) Fang, Z.; Suhua, H.; Xu, L.; Jian, F.; Qi, L.; Zhiwei, W.; Chuanchang, L.; Yuanlai, X. Adsorption Kinetics and Thermodynamics of Rare Earth on Montmorillonite Modified by Sulfuric Acid. *Colloids Surf. A Physicochem. Eng. Asp.* **2021**, *627*, 127063.

(28) Deng, Y.; Qian, X.; Wu, Y.; Ma, T.; Xu, X.; Li, J.; Wang, G.; Yan, Y. Effects of Ciprofloxacin on Eichhornia Crassipes Phytoremediation Performance and Physiology under Hydroponic Conditions. *Environmental Science and Pollution Research* **2022**, *29* (31), 47363–47372.

(29) Kuo, L.; Mallick, B. Variable Selection for Regression Models. *Sankhyā: The Indian Journal of Statistics, Series B* **1998**, 65–81.

(30) Zhang, X.; Li, Y.; Wu, M.; Pang, Y.; Hao, Z.; Hu, M.; Qiu, R.; Chen, Z. Enhanced Adsorption of Tetracycline by an Iron and Manganese Oxides Loaded Biochar: Kinetics, Mechanism and Column Adsorption. *Bioresour. Technol.* **2021**, *320*, 124264.

(31) Osmari, T. A.; Gallon, R.; Schwaab, M.; Barbosa-Coutinho, E.; Severo Jr, J. B.; Pinto, J. C. Statistical Analysis of Linear and Non-Linear Regression for the Estimation of Adsorption Isotherm Parameters. *Adsorption Science & Technology* **2013**, *31* (5), 433–458.

(32) Yin, Y.; Allen, H. E.; Huang, C. P.; Sanders, P. F. Adsorption/Desorption Isotherms of Hg (II) by Soil. *Soil Sci.* **1997**, *162* (1), 35–45.

(33) Tu, C.; Wei, J.; Guan, F.; Liu, Y.; Sun, Y.; Luo, Y. Biochar and Bacteria Inoculated Biochar Enhanced Cd and Cu Immobilization and Enzymatic Activity in a Polluted Soil. *Environ. Int.* **2020**, *137*, 105576.

(34) Mian, M. M.; Liu, G. Sewage Sludge-Derived TiO2/Fe/Fe3C-Biochar Composite as an Efficient Heterogeneous Catalyst for Degradation of Methylene Blue. *Chemosphere* **2019**, *215*, 101–114.

(35) Azizian, S. Kinetic Models of Sorption: A Theoretical Analysis. *J. Colloid Interface Sci.* **2004**, *276* (1), 47–52.

(36) Kumar, K. V.; Gadipelli, S.; Wood, B.; Ramisetty, K. A.; Stewart, A. A.; Howard, C. A.; Brett, D. J. L.; Rodriguez-Reinoso, F. Characterization of the Adsorption Site Energies and Heterogeneous Surfaces of Porous Materials. *J. Mater. Chem. A Mater.* **2019**, *7* (17), 10104–10137.

(37) Joy, J.; Krishnamoorthy, A.; Tanna, A.; Kamathe, V.; Nagar, R.; Srinivasan, S. Recent Developments on the Synthesis of Nanocomposite Materials via Ball Milling Approach for Energy Storage Applications. *Applied Sciences* **2022**, *12* (18), 9312.

(38) Maneechakr, P.; Karnjanakom, S. Adsorption Behaviour of Fe (II) and Cr (VI) on Activated Carbon: Surface Chemistry, Isotherm, Kinetic and Thermodynamic Studies. *J. Chem. Thermodyn.* **2017**, *106*, 104–112.

(39) Hao, Y.; Ma, H.; Wang, Q.; Zhu, C.; He, A. Complexation Behaviour and Removal of Organic-Cr (III) Complexes from the Environment: A Review. *Ecotoxicol. Environ. Saf.* **2022**, *240*, 113676.